Two-component model of the neutron diffuse scattering in the relaxor ferroelectric PZN-4.5%PT

Zhijun Xu,[1,2] Jinsheng Wen,[1,3] Guangyong Xu,[1] C. Stock,[4,5] J. S. Gardner,[4,5] and P. M. Gehring[5]
[1]*Condensed Matter Physics and Materials Science Department, Brookhaven National Laboratory, Upton, New York 11973, USA*
[2]*Department of Physics, City College of New York, New York, New York 10033, USA*
[3]*Department of Materials Science and Engineering, Stony Brook University, Stony Brook, New York 11794, USA*
[4]*Indiana University, 2401 Milo B. Sampson Lane, Bloomington, Indiana 47408, USA*
[5]*NIST Center for Neutron Research, National Institute of Standards and Technology, Gaithersburg, Maryland 20899, USA*
(Received 8 April 2010; revised manuscript received 23 September 2010; published 28 October 2010)

We report measurements of the neutron diffuse scattering in a single crystal of the relaxor ferroelectric material 95.5%$Pb(Zn_{1/3}Nb_{2/3})O_3$-4.5%$PbTiO_3$. Our results suggest that the nanometer scale structure in this compound exhibits both ⟨100⟩ and ⟨110⟩ polarizations, which contribute to different portions of the total diffuse scattering intensity. These contributions can be distinguished by the differing responses to an electric field applied along [001]. While diffuse scattering intensities associated with ⟨110⟩ (T2-type) polarizations show little to no change in a [001] field, those associated with ⟨100⟩ (T1-type) polarizations are partially suppressed by the field at temperatures below the Curie temperature $T_C \sim 475$ K. Neutron spin-echo measurements show that the diffuse scattering at (0.05,0,1) is largely dynamic at high temperature and gradually freezes on cooling, becoming mostly static at 200 K.

DOI: 10.1103/PhysRevB.82.134124 PACS number(s): 77.80.Jk, 61.05.fg

I. INTRODUCTION

The study of relaxors has grown dramatically over the past two decades. While many interesting properties distinguish relaxors from conventional ferroelectrics, the hallmark of relaxors is a highly frequency-dependent dielectric response that peaks broadly at a temperature that is unrelated to any structural phase transition.[1–3] Although the origin of many relaxor properties are still not well understood, most researchers tend to agree that the chemical short-range order in these materials, which are primarily compositionally disordered oxides, plays a key role in determining the bulk response.[4,5] In the case of the well-known lead-based, perovskite ABO_3 relaxors $Pb(Mg_{1/3}Nb_{2/3})O_3$ (PMN) and $Pb(Zn_{1/3}Nb_{2/3})O_3$(PNZ),[1,6] the mixture of 2^+ and 5^+ *B*-site cations leads to local charge imbalances that create random fields that destroy long-range polar order.[7–10] On the other hand short-range polar order, more commonly known as polar nanoregions (PNRs), appears at temperatures well above the temperature at which the dielectric susceptibility reaches a maximum (T_{max}).[11] There have been substantial experimental evidences exist that suggest the PNR influence various bulk properties of relaxors such as the thermal expansion in PMN,[12] the piezoelectric coefficients in PMN doped with $PbTiO_3$ (PMN-*x*PT),[13] and the transverse-acoustic (TA) phonon lifetimes in PZN doped with 4.5% $PbTiO_3$ (PZN-4.5%PT).[14] However, unlike the chemical short-range order, which is quenched and thus does not change with temperature, the polar short-range order (PNR) is sensitive to both temperature and external electric fields. It has therefore been the focus of numerous studies.

Different techniques including dielectric spectroscopy,[4,15] Raman scattering,[16–19] and piezoelectric force microscopy[20,21] have been used to explore the behavior of PNR in relaxor systems. Yet the most effective and direct probe of PNR within bulk relaxor samples is arguably obtained through measurements of the corresponding diffuse scattering, which reflects the presence of short-range ordered, atomic displacements.[22] Many neutron[10,23–31] and x-ray diffuse[32–34] scattering studies have been performed to determine the structure, polarization, and other properties of PNR. It has been shown that the diffuse scattering in pure PMN, PZN, and their solid solutions with low PT doping, exhibits very similar behavior.[13,35] In all cases the diffuse scattering intensities are strongly anisotropic, vary with Brillouin zone, and can be affected by an external electric field. Most neutron and x-ray diffuse scattering studies also agree that the diffuse scattering in both PMN-*x*PT and PZN-*x*PT systems extends preferentially along ⟨110⟩ in reciprocal space. This diffuse scattering is rod shaped but adopts an "X" or butterfly shape when measured in the (*HK*0) scattering plane near reflections of the form (*h*00). Detailed analysis indicates that the butterfly-shaped diffuse scattering is associated with short-range ordered, ionic displacements oriented along $\langle 1\bar{1}0 \rangle$ (Ref. 35) and couples strongly to TA phonons propagating along ⟨110⟩ (TA_2 modes).[14,36] For this reason we shall refer to it as "T2-diffuse scattering" in this paper. The T2-diffuse scattering intensities come from PNR composed of ionic displacements that are neither purely strain (no relative changes between the *A*, *B*, and O site positions) nor purely polar (only relative changes between *A*, *B*, and O site positions) in origin, which suggests that the local atomic structure both within and around the PNR is very complicated.[37] A number of important models deal with the PNR and other relaxor properties[38,39] as well as their possible chemical origins.[40–42] However the detailed local atomic structure of relaxor compounds is far from being fully understood at this point. In this paper, we will base our discussion on the so-called "pancake" model proposed in Refs. 14 and 35.

When an external electric field is applied along [111], the T2-diffuse scattering intensities are redistributed between different rods of diffuse scattering while the overall diffuse scattering intensity appears to be conserved [see panels (a)

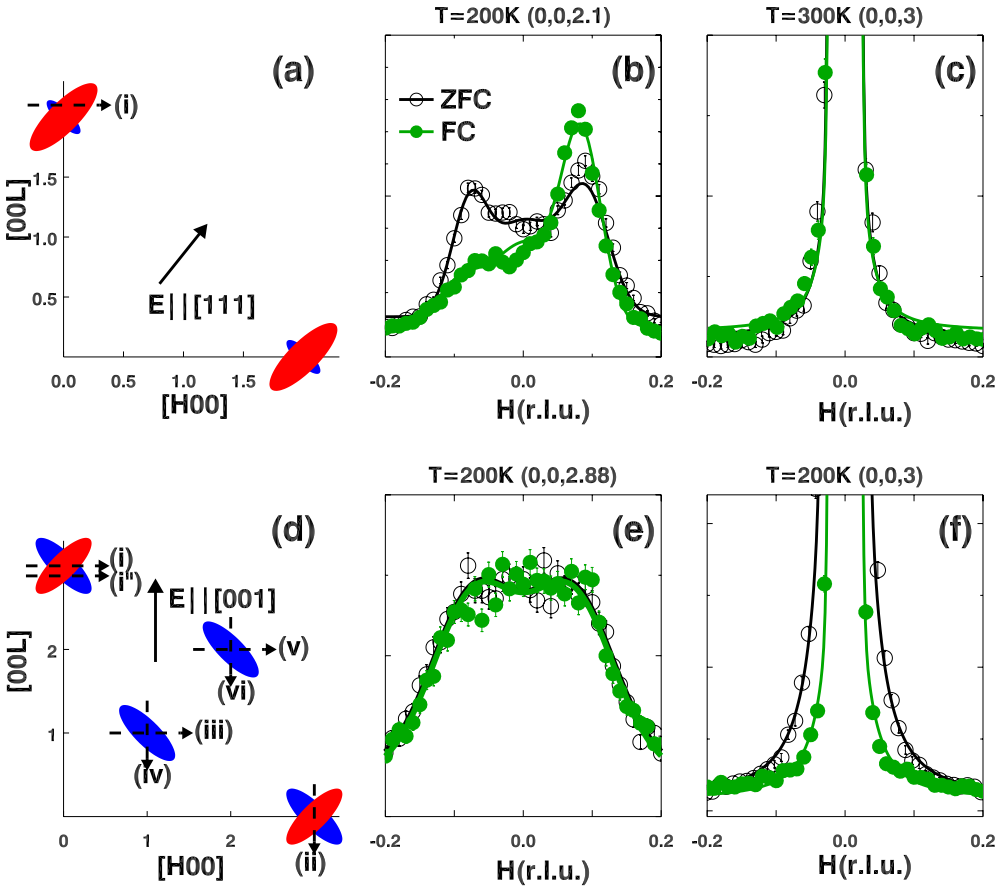

FIG. 1. (Color online) (a) Schematic of the neutron-scattering measurements made in the $(H0L)$ scattering plane with an electric field applied along [111]. The large (red) and small (blue) ellipses illustrate how the T2-diffuse scattering intensity is redistributed after the sample is FC. (b) Measurements of the diffuse scattering intensity near (002) [see scan (i) in panel (a)] at 200 K (data taken from Ref. 14). Scans were made along $(H,0,2.1)$ because they intercept both wings of the butterfly sufficiently far from (002) that significant contamination from unwanted Bragg peak scattering can be avoided, thus making it possible to monitor how intensities of the two wings change with field and temperature. Open circles represent ZFC data and closed circles represent FC data. (c) Transverse scan across (003) measured at 300 K on a PZN-8%PT. (d) Schematic identical to that in panel (a) except with the electric field applied along [001]. Dashed lines denote linear q scans measured across or near various Bragg peaks. (b) Measurements of the T2-diffuse scattering intensity near (003) [see scan (i″) in panel (d)] at 200 K. (f) Transverse scans at 200 K along [100] measured across (003) [see scan (i) in panel (d)]. Error bars represent the square root of the number of counts.

and (b) of Fig. 1].[34] However when an external field is applied along [001], the T2-diffuse scattering is essentially unchanged [see panel (e) of Fig. 1].[43] At the same time, we note that there is evidence that suggests the presence of another type of diffuse scattering that is distinct from the T2-diffuse scattering. In particular, Gehring *et al.*[44] found that the diffuse scattering measured in PZN-8%PT at 400 K along $(H03)$ is strongly suppressed by an external [001] field, whereas that measured along $(30L)$ is unaffected. These observations have been confirmed in our measurements on PZN-4.5%PT [see panel (f) of Fig. 1] and cannot be explained by a simple redistribution of the T2-diffuse scattering. We shall refer to this other type of diffuse scattering as T1-diffuse scattering.

We wish to emphasize here that the data presented in Fig. 1 cannot be understood in terms of a common origin of the diffuse scattering and geometric considerations. If the T1 and T2 diffuse scattering had a common origin, then a [001] field would have some effect on the T2 diffuse scattering measured at $(H,0,2.88)$. But our data clearly show that this is not the case. Whereas a [001] field has a strong effect on the T1 diffuse scattering measured near the Bragg peak [see panel (f) of Fig. 1], the same field has no measurable effect on the T2 diffuse scattering located further from the Bragg peak [see panel (e) of Fig. 1]. The converse is also true and is demonstrated experimentally in panels (b) and (c) of Fig. 1 while a [111] field has a substantial effect on the T2 diffuse scattering at $(H,0,2.1)$ [see panel (b) of Fig. 1], the same field has no effect on the T1 diffuse scattering measured near the Bragg peak [see panel (c) of Fig. 1]. Based on this analysis we can rule out a common origin for the T1 and T2 diffuse scattering components. We therefore assert that the origin of the two types of diffuse scattering must be different.

In this paper we report diffuse scattering measurements made under a [001]-oriented electric field on the relaxor ferroelectric PZN-4.5%PT at reduced wave vectors q offset from various Bragg peaks along $\langle 001 \rangle$ in the $(H0L)$ zone [refer to the dashed lines in panel (d) of Fig. 1]. We show

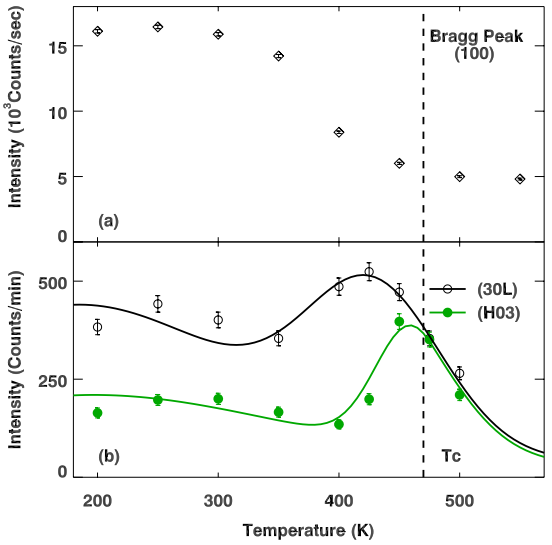

FIG. 2. (Color online) (a) (100) Bragg peak intensity versus temperature. The intensity increase near T_C is the result of a release of extinction at the phase transition. (b) Diffuse scattering intensity measured at (3,0,0.06) (open black symbols) and (−0.06,0,3) (closed green symbols) after cooling (FC) in a field E=4 kV/cm applied along [001]. The lines are guide to the eyes, and the error bars represent the square root of the number of counts.

that in addition to the T2-diffuse scattering, which dominates the total diffuse scattering intensity in most cases, there is a separate component of diffuse scattering that is primarily distributed along ⟨001⟩. The reason why we refer to this component as T1-diffuse scattering is because of its similarities in both polarization and propagation direction to that of T1 phonon modes in perovskite systems. The application of a [001] electric field has no obvious effect on the T1-diffuse scattering that is associated with short-range ordered, ionic displacements polarized along [100], but it strongly suppresses the diffuse scattering that is associated with short-range ordered, ionic displacements polarized along [001]. This effect is most prominent at temperatures slightly below $T_C \sim 475$ K. In addition, spin-echo measurements performed on the same sample show that the diffuse scattering has a large dynamic component at high temperature (550 K), which gradually freezes and becomes almost fully static at 200 K.

II. EXPERIMENTAL DETAILS

The sample used in our experiment is a PZN-4.5%PT single crystal. The crystal is rectangular with {100} cut surfaces and dimensions of $10\times10\times3$ mm^3. The sample has a cubic lattice spacing of a=4.05 Å at 300 K; thus 1 reciprocal lattice unit (r.l.u.) equals $2\pi/a$=1.55 Å^{-1}. Cr/Au electrodes were sputtered onto the two largest opposing crystal surfaces. The Curie temperature of this compound $T_C \sim 475$ K, which is accompanied by a strong release of extinction that is visible at the (100) Bragg peak and shown in panel (a) of Fig. 2. Neutron diffuse scattering measurements were performed on the BT-9 triple-axis spectrometer located at the NIST Center for Neutron Research (NCNR). We used horizontal beam collimations of 40′-47′-sample-40′-80′ and a fixed final neutron energy of 14.7 meV (λ=2.359 Å). Two pyrolytic graphite filters were placed before and after the sample to minimize the presence of neutrons with higher order wavelengths. An external electric field E=4 kV/cm was applied along [001] above 550 K during all of the field-cooled (FC) measurements.

Neutron spin-echo (NSE) measurements were performed on the NG-5 NSE spectrometer, also located at the NCNR. The experiment was performed at the scattering vector $\mathbf{Q}$=(0.05,0,1) ($|\mathbf{Q}|$=1.559 Å^{-1}) and at a neutron wavelength λ=5.5 Å for all time scales. The instrumental resolution was measured with the sample cooled to 40 K where all dynamical processes occurring on instrumentally accessible time scales are assumed to be frozen.

III. RESULTS AND DISCUSSION

A. Evidence of the T1-diffuse scattering component

Our study of the T1-diffuse scattering was conducted by performing a series of linear q scans, represented by the dashed arrows drawn in panel (d) of Fig. 1, under both FC and zero-field-cooled (ZFC) conditions around the (300), (003), (202), and (101) Bragg peaks. Diffuse scattering intensities measured at (3,0,0.06) and (−0.06,0,3) are plotted in panel (b) of Fig. 2. The temperature dependence similar to that reported for the T2-diffuse scattering in that the diffuse scattering increases with cooling and saturates at low temperature. The peak observed near T_C is most likely the result of the critical scattering that appears near the structural phase transition; similar behavior was observed by Stock *et al.* in PZN.[8] Linear q scans of the diffuse scattering intensity measured at 400 K under both FC and ZFC conditions are plotted in Fig. 3. It is immediately clear that the diffuse scattering intensities are suppressed around (003) after field cooling whereas no such change occurs around (300); this effect is also evident in panel (b) of Fig. 2. These results are consistent with those obtained previously on PZN-8PT.[44] At this point it is important to recall that the neutron diffuse scattering cross section resulting from correlated ionic displacements is proportional to $|\mathbf{Q}\cdot\boldsymbol{\epsilon}|^2$, where $\boldsymbol{\epsilon}$ is a unit vector along the displacement direction (for a more detailed discussion see Sec. III C). Therefore measurements of the diffuse scattering intensity made near (300) are mainly sensitive to short-range ordered ionic displacements oriented along [100] while those made near (003) reflect the presence of ordered ionic displacements oriented along [001]. The data shown in Fig. 3 therefore suggest that the short-range ordered ionic displacements oriented along [001] are significantly suppressed by an external electric field applied along [001]. This scattering is what we refer to as T1-diffuse scattering.

Mesh scans were also performed to map out the geometry of the diffuse scattering intensity distributions around various Bragg peaks under different conditions. The resulting intensity contours measured near (300) and (003) at 400 K are displayed in Fig. 4. The white, dashed lines shown in panels (c) and (d) of Fig. 4 are guide to the eyes that describe the shape of constant diffuse scattering intensity contours (which include both T1 and T2 components) under ZFC con-

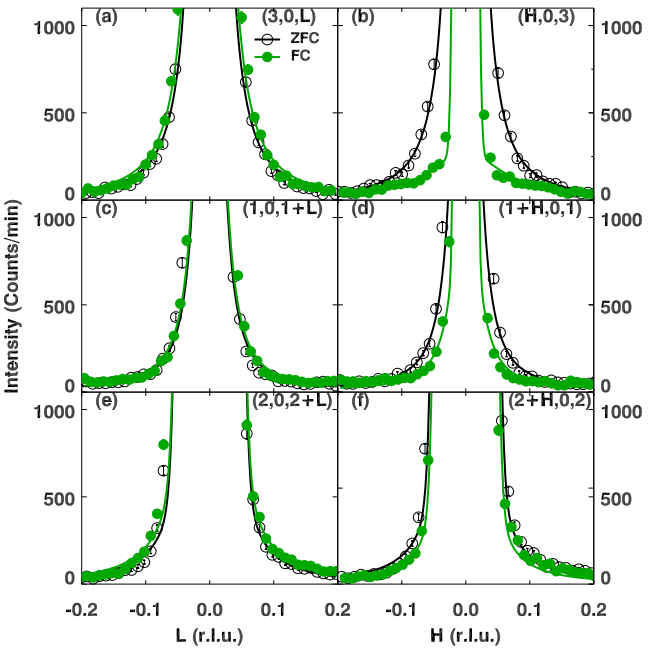

FIG. 3. (Color online) Diffuse scattering intensity measured at 400 K. ZFC data are shown as (black) open circles and FC data are shown as (green) closed circles. Data were taken around (a) $(3,0,L)$ [scan (ii) in panel (d) of Fig. 1]; (b) $(H,0,3)$ [scan (i) in panel (d) of Fig. 1]; (c) $(1,0,1+L)$ [scan (iv) in panel (d) of Fig. 1]; and (d) $(1+H,0,1)$ [scan (iii) in panel (d) of Fig. 1]. (e) $(2,0,2+L)$ [scan (v) of panel (d) in Fig. 1]; and (f) $(2+H,0,2)$ [scan (vi) of panel (d) in Fig. 1]. The solid lines are based on least-square fits to the data described in the text. The error bars represent the square root of the number of counts.

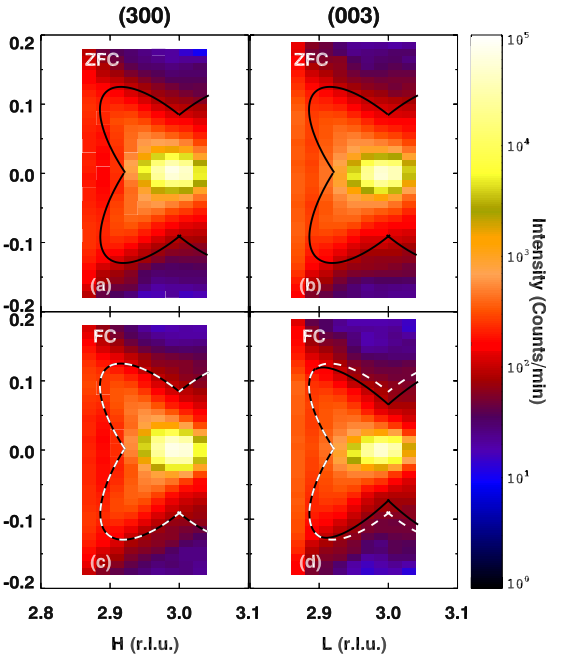

FIG. 4. (Color online) Contour maps of the diffuse scattering measured near (300) and (003) at 400 K under both ZFC and FC conditions. Mechanical constraints on the Q range on BT9 prevented us from measuring complete mesh scans at both (003) and (300). The solid and dashed lines are guide to the eyes.

ditions, as shown in panels (a) and (b). The corresponding intensity contour maps measured under FC conditions are shown in panels (c) and (d). Near (300), the FC mesh scan reveals a shape that is very similar to that obtained under ZFC conditions; however the one measured near (003) appears to be slightly narrower but only in the direction transverse ([100]) to the scattering vector $\mathbf{Q}=(003)$. This asymmetry is important because it implies that the T1-diffuse scattering associated with short-range ordered [001] ionic displacements is distributed primarily along the transverse direction ([100]) near (003) but not longitudinally (i.e., not along [001]). This is why we call this scattering "T1-diffuse scattering;" both its polarization and distribution in q space resemble that of the T1 phonon mode. On the other hand, the butterfly-shaped T2-diffuse scattering, which is strongly affected by an electric field applied along [111], is *not* affected by an electric field applied along [001]. Apparently the T2-diffuse scattering dominates the diffuse scattering intensity measured at most q values; the presence of the T1-diffuse scattering component only becomes evident through a change in its intensity once an external electric field is applied along [001].

Our measurements near (300) and (003) suggest that a [001]-oriented electric field can only reduce the diffuse scattering intensities associated with ionic displacements that are parallel to the field. To test this idea further, we studied the diffuse scattering intensity near (101) as well. Unlike the situation near (300) and (003), both [100]- and [001]-oriented atomic displacements/polarizations will contribute to the overall neutron diffuse scattering cross section near (101) because then $\mathbf{Q}\|[101]$. Linear scans made along the L ([001]) and H ([100]) directions near (101) are shown in panels (c) and (d) of Fig. 3. As shown in panel (d) of Fig. 3, the field suppresses the diffuse scattering intensity distributed along $\boldsymbol{q}\|[100]$, which must come from ionic displacements oriented along [001], as was the case for the T1-diffuse scattering measured near (003). By symmetry there must also be diffuse scattering associated with ionic displacements oriented along [100], which is distributed along $\boldsymbol{q}\|[001]$. However, as was the case near (300), this part of the T1-diffuse scattering is not affected by the external [001] field as is shown in panel (c) of Fig. 3. The measurements made near (202) show a similar trend but they exhibit a smaller field effect than do those made near (101).

These results suggest that the effects of an electric field on the diffuse scattering are rather complicated and cannot be simply understood as a rotation or alignment of the local ionic displacements. Consider, for instance, the effect of a [001]-oriented electric field on the T2-diffuse scattering. This field is perpendicular to two of the six $\langle 110\rangle$ directions ([110] and $[1\bar{1}0]$) but it has nonzero components along the other four. However, no effect on any portion of the T2-diffuse scattering by a [001]-oriented field has been observed. A [001]-oriented field, on the other hand, does affect the T1-diffuse scattering measured for q along [001]. In the case of a [111]-oriented electric field,[35] the T2 diffuse scattering resulting from polarizations perpendicular to the field is enhanced while the rest is reduced. The situation is not entirely

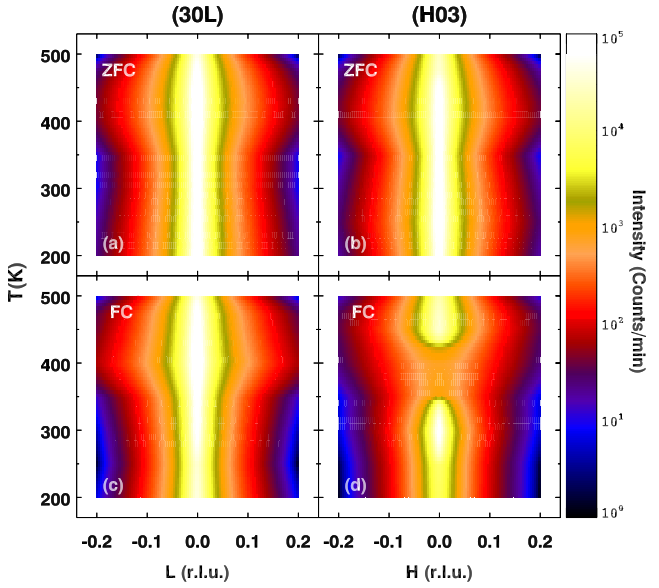

FIG. 5. (Color online) Contour maps of the fitted diffuse scattering intensities versus temperature along directions transverse to (300) and (003) under both ZFC and FC conditions.

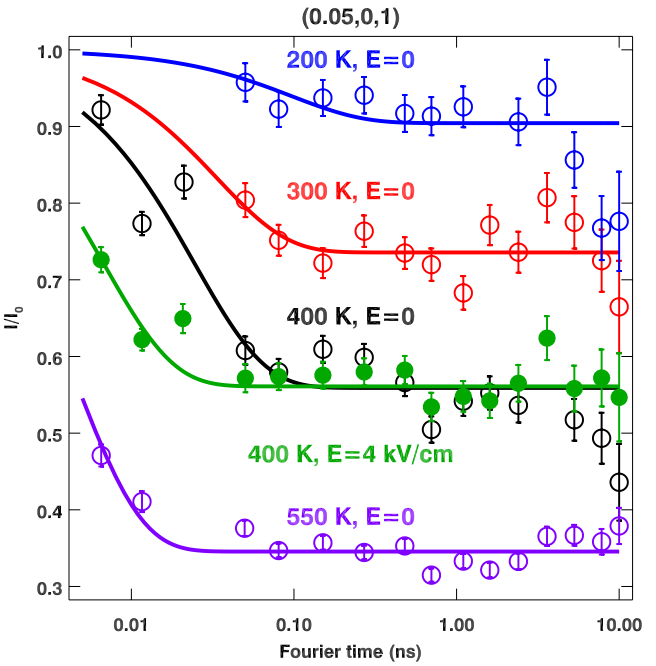

FIG. 6. (Color online) Neutron spin-echo data for different temperatures and electric field effect at 200 K (blue); 300 K (red); 400 K (black; green); and 550 K (purple). The error bars were determined from the square root of I and I_0. All data were taken under ZFC conditions shown with open circles except for the 400 K FC data shown with closed symbols. Lines are least-square fits to the databased on the model described in the text.

the same for a [001]-oriented field; it appears to reduce only the T1 diffuse scattering with polarization parallel to the field but it does not enhance any part of diffuse scattering with polarization perpendicular to the field. It is therefore reasonable to propose that the T1-diffuse scattering is a new component that is independent of the T2-diffuse scattering studied before, and its behavior under the influence of a [001]-oriented field should thus be understood via a different mechanism than that used to explain the way the T2-diffuse scattering changes under a [111] field.

The temperature dependence of the field-induced suppression of the T1-diffuse scattering is shown in Fig. 5. Transverse q scans across (300) and (003) were measured between 200 and 500 K. These scans were fit to a resolution-limited Gaussian function of q, used to describe the Bragg peak intensity, and a broad Lorentzian function of q, which describes the diffuse scattering intensity. In Fig. 5 only the fitted diffuse scattering intensities are plotted versus temperature and q and converted into color contour maps. There are only tiny differences between the ZFC [see panel (a)] and FC [see panel (c)] measurements made near (300); however the diffuse scattering intensities near (003) shown in panel (d) are strongly suppressed in the FC condition for $T<T_C$ compared to those measured under ZFC conditions [panel (b)]. This suppression seems to be largest for temperatures between T_C and ~400 K, and becomes less pronounced with cooling, but still persists to lower temperatures [also see Fig. 3(b)]. This can be understood if the PNR are more dynamic near 400 K, and therefore more easily affected by the field. With further cooling, the PNR gradually freeze and so become harder to influence through an external field at lower temperatures.

B. Static versus dynamic origin of the T1-diffuse scattering component

Another question that has yet to be answered is whether PNR have a static or dynamic origin. Previous work using cold neutron spectrometers, which provide significantly better energy resolution than do thermal neutron spectrometers, have shown that the onset of elastic (static) diffuse scattering occurs at much lower temperatures than previously believed, i.e., well below the Burns temperature T_d.[12,26,45–47] These results imply that at high temperature the diffuse scattering is (at least partially) dynamic in nature. In order to better probe the energy/time scale of the diffuse scattering, we have performed spin-echo measurements on the same PZN-4.5%PT single crystal at the reciprocal lattice point (0.05,0,1.0) at different temperatures. The diffuse scattering intensities shown in Fig. 6 have been corrected for the instrumental resolution and plotted in the form of $I(\mathbf{Q},t)/I_0(\mathbf{Q},0)$ versus Fourier time t. These intensity plots can in fact provide information on how much of the total diffuse scattering at this $\mathbf{Q}$ is static. One sees that at high temperature (T=550 K), the diffuse scattering intensity decays to $I/I_0 \lesssim 40\%$ within $\lesssim 0.01$ ns. In other words, less than 40% of the diffuse scattering is static while the rest of the intensity is dynamic in nature having a relaxation time less than 0.01 ns [see Eq. (1)], which corresponds to an energy half width of $\hbar\Gamma \gtrsim 0.066$ meV. On cooling the relative size of the static diffuse scattering component increases, which is consistent with freezing of the PNR. At 200 K, the diffuse scattering is almost completely static ($I/I_0 \gtrsim 90\%$). These results are qualitatively similar to those obtained on pure PMN by Stock *et al.*[45] In both systems, the diffuse scattering is partially dynamic at high temperatures above T_C, and becomes mostly static at temperatures low enough. The time scale obtained

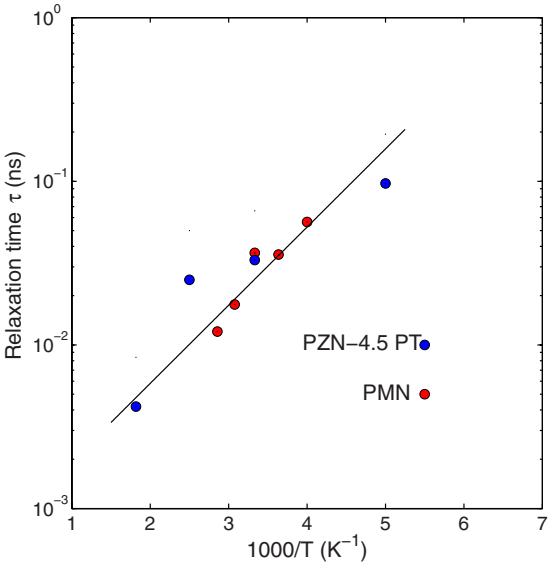

FIG. 7. (Color online) The relaxation time τ from neutron spin-echo measurements for PZN-4.5%PT (blue) and PMN (red from Ref. 45) plotted as a function of temperature. The solid line is a fit of PMN data to an Arrhenius law ($\tau=\tau_0 e^{U/k_BT}$) with $U=1100$ K.

from PZN-4.5%PT is also similar to those in PMN at low temperatures. However, at high temperature ($T=550$ K), we notice that the static fraction for diffuse scattering in PZN-4.5%PT is only about 35%, which is significantly smaller than that in PMN (about 50%) measured at 450 K. If we simply plot the relaxation times of PMN (from Ref. 45) and PZN-4.5%PT together as a function of temperature (see Fig. 7), we find that they seem to be in good agreement despite the difference in the values of T_C. However, if we just compare τ near T_C, we find that the relaxation time in PZN-4.5%PT ($\tau=0.025$ ns at $T=400$ K) is smaller than the value obtained for PMN ($\tau\approx 0.05$ ns at $T=250$ K). It is possible that the PNR become increasingly dynamic above T_C as more Ti is doped into the lattice; or this could simply be an intrinsic difference between the PMN and PZN systems.

We have also studied the effect of an external field along [001] on the diffuse scattering measured at 400 K. At (0.05,0,1) we should be sensitive to the T1-diffuse scattering associated with [001] ionic displacements, which should be partially suppressed by the [001] field. We find that, although the overall diffuse scattering intensity is reduced by the field, the static ratio I/I_0 at large Fourier times is not affected. However, the dynamic component decays much faster when the sample is FC compared to ZFC. The lines through the data shown in Fig. 6 are based on fits to a one parameter decay function

$$I(t)/I(0) = S + (1-S)\exp(-t/\tau). \quad (1)$$

In Table I, we list the temperature dependence of these parameters, including the static fraction S, the relaxation time τ, as well as the energy half width at half maximum (HWHM) $\hbar\Gamma=1/\tau$. At 400 K, $\tau\approx 0.025$ ns under ZFC conditions and $\tau\approx 0.0068$ ns under FC conditions. These τ values correspond to energy widths of $\hbar\Gamma\approx 0.027$ meV (ZFC) and $\hbar\Gamma\approx 0.10$ meV (FC), respectively.

Although we have obtained the relative fraction of the static portion of the diffuse scattering intensity in PZN-4.5%PT, it is clear that these spin-echo measurements do not provide the best time/energy scale to probe the relaxation time of the dynamic component of the diffuse scattering. To get better results one would need to perform measurements with energy resolution of about 20 μeV. Future measurements using the neutron backscattering technique are being planned for this purpose.

C. Short-range correlated ionic displacements associated with the T1-diffuse scattering

In general, the diffuse scattering intensity $I_{diff}(\mathbf{Q})$ coming from a single source at $\mathbf{Q}=\mathbf{G}+\mathbf{q}$ near the Bragg peak $\mathbf{G}$ can be approximately described by[37]

$$I_{diff}(\mathbf{Q}) = A|F_{diff}(\mathbf{G})|^2|f(\mathbf{q})|^2. \quad (2)$$

Here A is a scale factor. $|f(\mathbf{q})|^2$ is the Fourier transform of the real space shape of the PNR and describes the shape of the diffuse scattering intensity distribution around a Bragg peak. This term is in principle independent of Brillouin zone. $|F_{diff}(\mathbf{G})|^2$ is the diffuse scattering structure factor and is Brillouin zone dependent; it can be written as

$$|F_{diff}(\mathbf{G})|^2 = \left|\sum_i \mathbf{Q}\cdot\xi_i b_i \exp(-W_i)\exp(i\mathbf{G}\cdot\mathbf{R}_i)\right|^2, \quad (3)$$

where ξ_i, b_i, and R_i are the ionic displacement vector, neutron scattering length, and the lattice position of the ith atom in the unit cell, respectively, and $\exp(-W_i)$ is the Debye-Waller factor.

Many sources contribute to the total neutron diffuse scattering cross section in relaxors. In the case of PZN-4.5%PT these include six ⟨110⟩ polarization directions and three ⟨001⟩ polarization directions associated with the T2 and T1-diffuse scattering cross sections, respectively. It is very difficult to determine the absolute intensity of the T1-diffuse scattering directly because it coexists with the much stronger T2-diffuse scattering. However, we have shown that a [001]-oriented electric field can suppress portion of the T1-diffuse scattering intensity that is specifically associated with [001]-

TABLE I. Values of the fitting parameters used in Eq. (1). The energy width (HWHM) is calculated from $E=\hbar\Gamma=\hbar/\tau$.

	550 K	FC 400 K	ZFC 400 K	300 K	200 K
Static fraction S (%)	35	56	56	74	90
Relaxation time (τ) (ns)	0.0042	0.0068	0.025	0.033	0.097
Energy width E (meV)	0.16	0.1	0.027	0.02	0.007

TABLE II. Values for $|\mathbf{Q}\cdot\boldsymbol{\epsilon}|^2$ and the difference (ZFC-FC) of the T1-diffuse scattering intensity measured at $(3+q,0,0)$, $(2+q,0,2)$, and $(1+q,0,1)$ for $q=0.06$ r.l.u..

	(300)	(202)	(101)
$\|\mathbf{Q}\cdot\boldsymbol{\epsilon}\|^2$	9	4	1
500 K	13	4	9
400 K	320	72	115
300 K	154	1	67
200 K	193	0	75

TABLE IV. Values for $|\mathbf{Q}\cdot\boldsymbol{\epsilon}|^2$ and the T2-diffuse scattering intensity measured at $(3-q,0,-q)$, $(2+q,0,2-q)$, and $(1+q,0,1-q)$ for $q=0.1$ r.l.u..

	(300)	(202)	(101)
$\|\mathbf{Q}\cdot\boldsymbol{\epsilon}\|^2$	9	8	2
500 K	243	144	125
400 K	342	262	163
300 K	409	525	191
200 K	519	762	216

oriented ionic displacements while leaving that associated with [100] and [010] ionic displacements (and the T2-diffuse scattering) unaffected. One can then exploit this fact and measure the change in the T1-diffuse scattering cross section in different Brillouin zones to determine the corresponding structure factor and solve for the relative magnitudes of the ionic shifts that contribute to the T1-diffuse scattering. If one assumes that the Debye-Waller factor does not vary appreciably with Brillouin zone, then one can simplify Eq. (3) to[23]

$$|F_{diff}(\mathbf{G})|^2 \propto |\mathbf{Q}\cdot\boldsymbol{\epsilon}|^2 \left| \sum_i b_i \cdot \xi_i \exp(i\mathbf{G}\cdot\mathbf{R}_i) \right|^2, \qquad (4)$$

where, again, $\boldsymbol{\epsilon}$ is the unit vector along the ionic displacement (polarization) direction.

As discussed in Sec. III A, the T1-diffuse scattering associated with short-range ordered, [001]-oriented, ionic displacements is distributed along [100] across each Bragg peak in the $(H0L)$ plane. We therefore chose to measure T1-diffuse scattering intensities at the reciprocal lattice positions $(q,0,3)$, $(1+q,0,1)$, and $(2+q,0,2)$. The differences between ZFC and FC measurements made at $q=0.06$ r.l.u., shown in Table II, are then used as the relative structure factors for the T1-diffuse scattering cross section. Here we have assumed that the electric field does not affect the structure factors. This is equivalent to the assumption that the electric field reduces the T1-diffuse scattering uniformly independent of Brillouin zone. Knowing $|F_{diff}(\mathbf{G})|^2$ at different Bragg peaks, one can solve for the average Pb, Zn/Nb/Ti, and O displacements in the unit cell that contribute to the T1-diffuse scattering. Similar to what was done in Ref. 37, we neglect any possible distortion or rotation of the oxygen octahedra and assume that all six oxygen atoms in one unit cell move as a unit. The relative ionic shifts that contribute to the T1-diffuse scattering intensities are listed in Table III. In Table III we have decomposed these ionic shifts into different components, i.e., one acoustic/strain component that corresponds to the uniform phase shift in which all atoms in the unit cell move together,[25] and two optic components that correspond to the Slater and Last modes[37,48] where the atoms in the unit cell only move relative to each other with no change in the center of mass. Apparently, as was the case for the T2-diffuse scattering, the local ionic displacements that give rise to the T1-diffuse scattering also consist of both acoustic/strain and optic/polar components.

We have also examined the T2-diffuse scattering intensity by making measurements at reduced wave vectors $q\|[110]$ offset from various Bragg peaks. The structure factors and ionic displacements contributing to the T2-diffuse scattering obtained from our PZN-4.5%PT sample are listed in Tables IV and V. We can therefore compare the local ionic structures that give rise to the T1-diffuse scattering to those that produce the T2-diffuse scattering. We find that the ionic displacements associated with the T1-diffuse scattering have a larger optic component; note that the shifts for the Zn/Nb/Ti site associated with the T1-diffuse scattering are larger than those associated with the T2-diffuse scattering in Ref. 37. Previous work has shown that the T2-diffuse scattering is coupled strongly to transverse-acoustic phonons and strains in relaxor systems[14,36] but not with the soft transverse-optic (TO) phonon. We expect that this situation could be different for the T1-diffuse scattering, which may in fact couple more strongly to the soft TO phonon because it has a larger optic component. This will of course need to be verified by future experiments.

IV. SUMMARY

Our neutron-scattering measurements clearly show that in addition to the well-known butterfly-shaped diffuse scatter-

TABLE III. Calculated T1-type ionic displacements and relative magnitudes of different modes. All displacements have been normalized to that for the Pb cation. The values for the Slater, Last, and shift modes are based on the oxygen octahedra displacements.

	δ_{Pb}	$\delta_{Zn,Nb}$	δ_O	Shift	Slater	Last
500 K	1.0	0.86	−0.51	0.75	−0.84	−0.41
400 K	1.0	0.54	−0.39	0.69	−0.58	−0.51
300 K	1.0	0.73	−0.73	0.69	−0.91	−0.52
200 K	1.0	0.69	−0.78	0.67	−0.91	−0.54

TABLE V. Calculated T2-type ionic displacements and relative magnitudes of different modes. All displacements have been normalized to that for the Pb cation. The values for the Slater, Last, and shift modes are based on the oxygen octahedra displacements.

	δ_{Pb}	$\delta_{Zn,Nb}$	δ_{O}	Shift	Slater	Last
500 K	1.0	0.06	−0.22	0.61	−0.18	−0.65
400 K	1.0	0.03	−0.17	0.61	−0.12	−0.65
300 K	1.0	0.02	−0.07	0.62	−0.06	−0.63
200 K	1.0	−0.03	−0.02	0.61	0.00	−0.63

ing, a second, distinct, diffuse scattering component also exists in the PZN-*x*PT relaxor system. This so-called T1-diffuse scattering can be differentiated from the butterfly-shaped T2-diffuse scattering through its dependence on a ⟨001⟩-oriented electric field. Quantitative analysis of the short-range ordered, ⟨001⟩-oriented, ionic displacements associated with the T1-diffuse scattering suggest that both acoustic/strain and optic/polar ionic displacements are present, a situation that is very similar to that for the T2-diffuse scattering. Spin-echo measurements also show that the diffuse scattering cross section exhibits a large dynamic component at high-temperature paraelectric phase above T_C and gradually freezes, becoming almost entirely static for temperatures well below T_C in the ferroelectric phase.

The electric field dependence of the T1 and T2-diffuse scattering cross sections are quite different; this implies that they might originate from independent nanoscale polar structures. On the other hand, they are very similar in many other aspects: both exhibit strain/polar components and both freeze with cooling. This raises another scenario in which the two diffuse scattering components might be associated within different ⟨001⟩ and ⟨110⟩ components of the ionic displacements with the same nanoscale polar structure. The average local atomic shifts in these nanoscale structures could very well be along other directions, e.g., along ⟨111⟩ directions as suggested by neutron pair distribution function measurements from PMN.[30] The neutron diffuse scattering intensities that we observe here arise only from one or more components of these local displacements that become spatially short-range ordered. Any components of atomic displacements that are entirely disordered will only contribute to the overall background and will not affect the diffuse scattering intensities discussed in this work. Our data do not allow us to determine definitively which scenario is correct, thus more detailed studies are clearly required. However, our results do strongly suggest that when studying PNR in relaxor systems, the existence of complex nanoscale polar structures composed of both ⟨001⟩ and ⟨110⟩-oriented ionic displacements will have to be carefully taken into consideration; indeed, these may affect the lifetimes of phonons propagating along these two sets of directions.

ACKNOWLEDGMENTS

We wish to thank W. Ratcliff, S. M. Shapiro, and S. B. Vakhrushev for useful discussions. Financial support from the U.S. Department of Energy under Contract No. DE-AC02-98CH10886 and the Natural Sciences and Engineering Research Council of Canada (NSERC) is also gratefully acknowledged.

[1] S. E. Park and T. R. Shrout, J. Appl. Phys. **82**, 1804 (1997).
[2] K. Uchino, *Piezoelectric Actuators and Ultrasonic Motors* (Kluwer, Dordrecht, 1996).
[3] R. F. Service, Science **275**, 1878 (1997).
[4] L. E. Cross, Ferroelectrics **76**, 241 (1987).
[5] B. P. Burton, E. Cockayne, S. Tinte, and U. V. Waghmare, Phase Transitions **79**, 91 (2006).
[6] J. Kuwata, K. Uchino, and S. Nomura, Ferroelectrics **37**, 579 (1981).
[7] W. Kleemann and R. Lindner, Ferroelectrics **199**, 1 (1997).
[8] C. Stock, R. J. Birgeneau, S. Wakimoto, J. S. Gardner, W. Chen, Z. G. Ye, and G. Shirane, Phys. Rev. B **69**, 094104 (2004).
[9] C. Stock, D. Ellis, I. P. Swainson, G. Xu, H. Hiraka, Z. Zhong, H. Luo, X. Zhao, D. Viehland, R. J. Birgeneau, and G. Shirane, Phys. Rev. B **73**, 064107 (2006).
[10] S. N. Gvasaliya, S. G. Lushnikov, and B. Roessli, Phys. Rev. B **69**, 092105 (2004).
[11] G. Burns and F. H. Dacol, Phys. Rev. B **28**, 2527 (1983).
[12] P. M. Gehring, H. Hiraka, C. Stock, S. H. Lee, W. Chen, Z. G. Ye, S. B. Vakhrushev, and Z. Chowdhuri, Phys. Rev. B **79**, 224109 (2009).
[13] M. Matsuura, K. Hirota, P. M. Gehring, Z.-G. Ye, W. Chen, and G. Shirane, Phys. Rev. B **74**, 144107 (2006).
[14] G. Xu, J. Wen, C. Stock, and P. M. Gehring, Nature Mater. **7**, 562 (2008).
[15] E. V. Colla, N. K. Yushin, and D. Viehland, J. Appl. Phys. **83**, 3298 (1998).
[16] A. M. Welsch, B. Mihailova, M. Gospodinov, R. Stosch, B. Guttler, and U. Bismayer, J. Phys.: Condens. Matter **21**, 235901 (2009).
[17] H. Ohwa, M. Iwata, N. Yasuda, and Y. Ishibashi, Jpn. J. Appl. Phys., Part 1 **37**, 5410 (1998).
[18] H. Ohwa, M. Iwata, N. Yasuda, and Y. Ishibashi, Ferroelectrics **229**, 147 (1999).
[19] I. G. Siny, E. Husson, J. M. Beny, S. G. Lushnikov, E. A. Rogacheva, and P. P. Syrnikov, Ferroelectrics **248**, 57 (2000).

[20] P. Lehnen, W. Kleemann, T. Woike, and R Pankrath, Phys. Rev. B **64**, 224109 (2001).
[21] V. V. Shvartsman and A. L. Kholkin, Phys. Rev. B **69**, 014102 (2004).
[22] G. Xu, J. Phys. Soc. Jpn. **79**, 011011 (2010).
[23] G. Xu, Z. Zhong, Y. Bing, Z.-G. Ye, C. Stock, and G. Shirane, Phys. Rev. B **70**, 064107 (2004).
[24] S. B. Vakhrushev, A. A. Naberezhnov, N. M. Okuneva, and B. N. Savenko, Phys. Solid State **37**, 1993 (1995).
[25] K. Hirota, Z. G. Ye, S. Wakimoto, P. M. Gehring, and G. Shirane, Phys. Rev. B **65**, 104105 (2002).
[26] H. Hiraka, S. H. Lee, P. M. Gehring, G. Xu, and G. Shirane, Phys. Rev. B **70**, 184105 (2004).
[27] J. Hlinka, S. Kamba, J. Petzelt, J. Kulda, C. A. Randall, and S. J. Zhang, J. Phys.: Condens. Matter **15**, 4249 (2003).
[28] D. La-Orauttapong, J. Toulouse, Z.-G. Ye, W. Chen, R. Erwin, and J. L. Roberston, Phys. Rev. B **67**, 134110 (2003).
[29] B. Dkhil, J. M. Kiat, G. Calvarin, G. Baldinozzi, S. B. Vakhrushev, and E. Suard, Phys. Rev. B **65**, 024104 (2001).
[30] I. K. Jeong, T. W. Darling, J. K. Lee, T. Proffen, R. H. Heffner, J. S. Park, K. S. Hong, W. Dmowski, and T. Egami, Phys. Rev. Lett. **94**, 147602 (2005).
[31] C. Stock, G. Xu, P. M. Gehring, H. Luo, X. Zhao, H. Cao, J. F. Li, D. Viehland, and G. Shirane, Phys. Rev. B **76**, 064122 (2007).
[32] H. You and Q. M. Zhang, Phys. Rev. Lett. **79**, 3950 (1997).
[33] N. Takesue, Y. Fujii, and H. You, Phys. Rev. B **64**, 184112 (2001).
[34] G. Xu, Z. Zhong, Y. Bing, Z. G. Ye, and G. Shirane, Nature Mater. **5**, 134 (2006).
[35] G. Xu, Z. Zhong, H. Hiraka, and G. Shirane, Phys. Rev. B **70**, 174109 (2004).
[36] C. Stock, H. Luo, D. Viehland, J. F. Li, I. P. Swainson, R. J. Birgeneau, and G. Shirane, J. Phys. Soc. Jpn. **74**, 3002 (2005).
[37] G. Xu, P. M. Gehring, and G. Shirane, Phys. Rev. B **74**, 104110 (2006).
[38] M. Paściak, M. Wołcyrz, and A. Pietraszko, Phys. Rev. B **76**, 014117 (2007).
[39] I. Grinberg, Y.-H. Shin, and A. M. Rappe, Phys. Rev. Lett. **103**, 197601 (2009).
[40] T. R. Welberry, M. J. Gutmann, D. H. Woo, J. Goossens, G. Xu, C. Stock, W. Chen, and Z.-G. Ye, J. Appl. Crystallogr. **38**, 639 (2005).
[41] T. R. Welberry, D. J. Goossens, and M. J. Gutmann, Phys. Rev. B **74**, 224108 (2006).
[42] B. P. Burton, E. Cockayne, and U. V. Waghmare, Phys. Rev. B **72**, 064113 (2005).
[43] J. Wen, G. Xu, C. Stock, and P. M. Gehring, Appl. Phys. Lett. **93**, 082901 (2008).
[44] P. M. Gehring, K. Ohwada, and G. Shirane, Phys. Rev. B **70**, 014110 (2004).
[45] C. Stock, L. Van Eijck, P. Fouquet, M. Maccarini, P. M. Gehring, G. Xu, H. Luo, X. Zhao, J. F. Li, and D. Viehland, Phys. Rev. B **81**, 144127 (2010).
[46] B. E. Vugmeister, Phys. Rev. B **73**, 174117 (2006).
[47] G.-M. Rotaru, S. N. Gvasaliya, B. Roessli, S. Kojima, S. G. Lushnikov, and P. Gunter, Appl. Phys. Lett. **93**, 032903 (2008).
[48] G. Shirane, J. D. Axe, and J. Harada, Phys. Rev. B **2**, 155 (1970).